

Assessment of Density Functional Theory in Studying on the Transition States of A Diiron-mediated N–N Bond Cleavage Reaction

Hang Yu¹, Qiongyao Zhang², Jing Xu², Xingbao Wang³, and Lun Luo²

¹Shenyang Aerospace University

²Hubei University of Medicine

³Taiyuan University of Technology

July 1, 2020

Abstract

The structure of transition state is very significant to further understand the related reaction system auxiliary N–N bond cleavage process. Here, in order to sort out some DFT functionals in searching the transition states in a N–N bond cleavage reaction mediated by the diiron complexes, compare the 45 density functionals with benchmark data of MP2 and DLPNO-CCSD(T) methods. By analyzing the structures and relative energies, we have found that four HGGGA functionals (B1B95, mPW1PBE, HSE1PBE, HSEh1PBE) are the more consistently reliable methods. And the B1B95 functionals provide the most reliable energetic properties within 3 kcal/mol of the data of DLPNO-CCSD(T) method.

Introduction

The aspire interest for elucidating the mechanism of the biological transformation of nitrogen to ammonia has lasted for more than 50 years.^[1] Much effort has been spent on understanding the conversion process from N₂ to NH₃ in which N-N bond cleavage is a key step in biological systems,^[2] and great progress has been made in this framework. But the biological nitrogen fixation process is so complicated that it is hard to directly obtain related mechanistic information in detail which is one reason that the limited experimental knowledge and methods. A powerful approach to elucidate the mechanism of N-N bond cleavage related to nitrogen fixation in nitrogenase or nitrogenase mimics is theoretical calculation, which is not only well-suited for the experimental observations on the mechanisms but also useful to obtain deeper insight into the mechanisms of this reaction. So a series of computational studies have been reported to have focused on the binding of N₂ to iron-sulfur clusters modeling FeMoco and their electronic properties.^[3] As far as we aware, there are still lack of systematic studies on the effects of DFT functionals for Fe₂S₂-based reactions. Kastner and Blochl^[3i] recently reported that the reduction of N₂ to NH₃ at the Fe sites of FeMoco favorably use the gradient corrected PBE^[4]functional. The QM and QM/MM models for the FeMoco of nitrogenase reported by Cao and co-workers^[3j] were employed generalized gradient approximation Perdew-Wang functional (PW91).^[5a] These results may suggest that using various functionals. So choosing suitable density functional is a problem. For example, previous studies on diiron complexes,^[6] we have discussed the complex Cp^{*}Fe(μ -SEt)₂(μ -NHNH₃)FeCp^{*} (Cp^{*} = η^5 -C₅Me₅, **1**) decomposed to Cp^{*}Fe(μ -SEt)₂(μ -NH)FeCp^{*} (**2**) and NH₃ (Scheme 1). Although using TPSSSTPSS^[7] functional has reproduced well the X-Ray structures, we could not locate transition state for the N-N bond cleavage. In general, the N-N bond cleavage is very significant to further understand the biological nitrogen fixation process. Therefore, gaining the transition states of N-N bond cleavage is significantly necessary.

In view of this, a key goal of this effort is to determine which DFT functionals with a moderate-sized basis set are able to search the transition states of the N-N bond cleavage of good quality for the larger systems of experimental and theories interest.

Hosted file

image1.emf available at <https://authorea.com/users/338325/articles/464354-assessment-of-density-functional-theory-in-studying-on-the-transition-states-of-a-diiron-mediated-n-n-bond-cleavage-reaction>

Scheme 1. The reaction (transformation from **1** to **2**) of N-N bond cleavage process.

Computational Details

All DFT and MP2^[8] geometry optimizations and vibrational calculations were carried out using the Gaussian 09 program package.^[9] As reported previously,^[6c] both complexes **1** and **2** were calculated to be the singlet ground state. Therefore, only singlet state was considered for the complexes involved in this system. The 6-31G* basis set was used for C, H, N and S atoms, and Fe atoms were treated by 6-311G* basis set. Each optimized structure was analyzed by harmonic vibrational frequencies obtained at the same level and characterized as a minimum ($N_{\text{imag}} = 0$) or a transition state ($N_{\text{imag}} = 1$). The transition state structures were shown to connect the reactant and product on either side via intrinsic reaction coordinate (IRC) following. Some relaxed potential energy scans of 18 functionals were performed with only the scanned N-N distance from 0.500 Å to 2.500 Å with stepsize 0.050 Å. The most reliable available levels, the domain-based local pair natural orbital coupled cluster method with single and double excitations and perturbative triple corrections (DLPNO-CCSD(T))^[10,11]/6-311G*(Fe)/6-31G*(C, H, N, S) in conjunction with the correlation fitting auxiliary basis set TZV/C for the single-point energy calculations were performed for the species at the MP2 optimized geometries in ORCA Program^[12] as the benchmark data. Considered the calculation of DLPNO-CCSD(T), the model compounds CpFe(μ -SMe)₂(μ -NHNH₃)FeCp (Cp = η^5 -C₅H₅, **1m**) and CpFe(μ -SMe)₂(μ -NH)FeCp (**2m**) (Figure 1) were adopted in this systems. The ONIOM calculations^[13] were carried out for **1** and **2** to validate the rationality of simplified model (in Supporting Information).

Hosted file

image2.emf available at <https://authorea.com/users/338325/articles/464354-assessment-of-density-functional-theory-in-studying-on-the-transition-states-of-a-diiron-mediated-n-n-bond-cleavage-reaction>

Figure 1 . Optimized structure of **1m** and **2m** at the B3LYP/6-311G*(Fe)/6-31G*(C, H, N, S) level.

Results and Discussion

Various density functionals were applied, including generalized-gradient approximation (GGA), hybrid GGA (HGGA), and long-range-separated hybrid GGA methods (LR-HGGA) (see Table 2 for the details).

In the process of search of transition states using various DFT methods, only 27 kinds of DFT methods (B3LYP, M06-2X, B3PW91, B1B95, mPW1PW91, mPW1LYP, mPW1PBE, B98, B971, B972, PBE1PBE, O3LYP, BMK, M06, tHCTHhyb, HSEh1PBE, HSE1PBE, wB97XD, wB97X, CAM-B3LYP, VSXC, HCTH93, HCTH147, HCTH(407), tHCTH, M06-L, TPSSh) got successfully the structures of transition states. However, attempts to locate a transition state for the cleavage of a N-N in **1m** of the other 18 kinds of functionals were unsuccessful. A relaxed scan of the N-N distance in **1m** indicates that the energy decreases monotonously as the N-N distance increases from 0.5 Å to 2.5 Å (Figure S1). These results suggest that cleavage of the N-N bond in **1m** is unlikely to occur. So these methods can't be discussed as follows.

Optimized Geometries

Firstly, we examined the geometries of stationary points (including reactant, transition state and product) along the reaction coordinate of the reaction of diiron-mediated N-N bond cleavage. The resulting selected framework geometry parameters are collected in Table S2-S4. A wide range of DFT functionals were used

for the benchmark study, including local, gradient-corrected, hybrid exchange-correlation, and long-range functionals. The *RMSE* (root mean square error) and R^2 (the

Table 2 . Benchmarked DFT functionals.

functional	type	refs
BP86	GGA	[14a, 14b]
HCTH93	GGA	[15]
HCTH147	GGA	[15]
HCTH(407)	GGA	[15]
B97D	GGA	[16]
PBEPBE	GGA	[4]
BLYP	GGA	[14a,17]
mPWPW91	GGA	[18]
PW91PW91	GGA	[5]
VSXC	GGA	[19]
tHCTH	GGA	[20]
TPSSTPSS	GGA	[7]
M06-L	GGA	[21]
PBE1PBE	HGGA	[4]
B3LYP	HGGA	[14a, 17, 22, 23]
B3PW91	HGGA	[14c, 24]
B3P86	HGGA	[14b, 14c]
mPW1PW91	HGGA	[18]
mPW1PBE	HGGA	[4, 18]
mPW1LYP	HGGA	[18, 18]
mPW3PBE	HGGA	[4, 18]
B98	HGGA	[23]
B971	HGGA	[15]
B972	HGGA	[25]
B1LYP	HGGA	[17, 26]
O3LYP	HGGA	[17, 27]
X3LYP	HGGA	[14a, 17, 24, 28]
BHandH	HGGA	[14a, 17]
BHandLYP	HGGA	[14a, 17]
HSEh1PBE	HGGA	[29]
HSE2PBE	HGGA	[30]
HSE1PBE	HGGA	[31]
PBEh1PBE	HGGA	[4, 32]
B1B95	HGGA	[14a, 27]
BMK	HGGA	[33]
M06	HGGA	[21a, 34]
M06-2X	HGGA	[21a, 34]
M06HF	HGGA	[21a, 35]
TPSSh	HGGA	[36]
tHCTHhyb	HGGA	[37]
wB97	LR-HGGA	[23b, 38]
wB97X	LR-HGGA	[38]
wB97XD	LR-HGGA	[23b, 39]
LC-wPBE	LR-HGGA	[40]
CAM-B3LYP	LR-HGGA	[41]

square of correlation coefficient) of structures were used to evaluate the performance of DFT functionals versus the higher level MP2 results, shown in Figure 2, respectively, using the following expressions:

(similarly hereinafter).

, where , , and are the values of MP2 method , that of the related DFT method, the mean of 's, and the mean of 's, respectively; $N = 8$ for reactant and transition state, $N = 7$ for product (similarly hereinafter).

It is generally known that the R^2 more close 1 illustrates the data closer to the standard value while the $RMSE$ value smaller data closer to the standard value. As shown in Figure 2a, for **1m**, the values of R^2 are greater than 0.920 (except for B972 method with $R^2 = 0.783$). The functionals perform in the following order based on the $RMSE$ errors:

(a) group 1 ($RMSE$ [0.064 Å, 0.077 Å]): B1B95, PBE1PBE, mPW1PBE, HSEh1PBE, HSE1PBE, mPW1PW91, tHCTHhyb, M06, tHCTH, TPSSh;

(b) group 2 ($RMSE$ [0.081 Å, 0.098 Å]): wB97XD, CAM-B3LYP, O3LYP, HCTH147, HCTH(407), B971, B98, HCTH93, M06-L, B3LYP;

(c) group 3 ($RMSE$ [0.103 Å, 0.400 Å]): mPW1LYP, VSXC, BMK, B3PW91, M06-2X, wB97X, B972.

This indicates that several functionals (group 1) yield convincing structures with $RMSE$ as small as 0.064 Å in case of the B1B95 functional. It is observed that most of the conventional hybrids including 9 HGGAs lie in this group as well as a GGA functional (tHCTH). The functionals in group 2 yield relatively good structures and the group consists of a collection of 4 GGAs, 4 HGGAs, and two LR-HGGAs (wB97XD, CAM-B3LYP). For group 3, which exhibits the $RMSE$ greater than 0.100 Å, consists of one GGA (VSXC), one LR-HGGA (wB97X), and 5 HGGAs. From these investigations, it is apparent that all of the functionals designated in group 1 are suitable to reproduce the MP2 results.

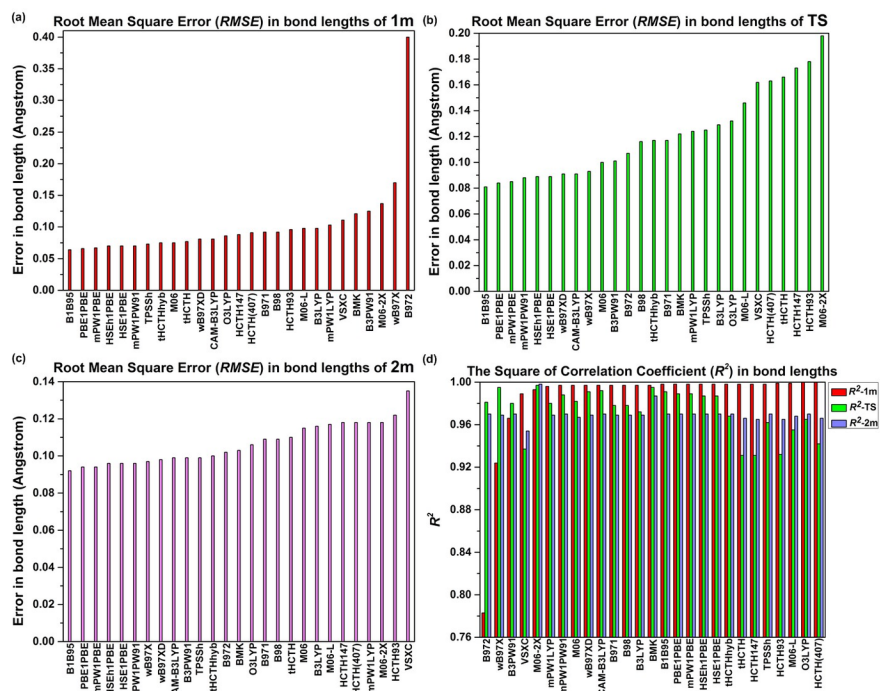


Figure 2 . The $RMSE$ in the framework bond lengths (including Fe–Fe, Fe–S, Fe–N and N–N bond length, Å) compared with the results of MP2 for **1m** (a), **TS** (b) and **2m** (c), respectively; and R^2 (d) in bond

lengths.

For transition state (**TS**) of N–N bond cleavage, shown in Figure 2b, the values of R^2 are greater than 0.930. The functionals perform in the following order along the *RMSE* errors:

(a) group 1 (*RMSE* [0.081 Å, 0.089 Å]): B1B95, PBE1PBE, mPW1PBE, mPW1PW91, HSEh1PBE, HSE1PBE;

(b) group 2 (*RMSE* [0.091 Å, 0.093 Å]): wB97XD, CAM-B3LYP, wB97X;

(c) group 3 (*RMSE* [0.100 Å, 0.198 Å]): M06, B3PW91, B972, B98, tHCTHhyb, B971, BMK, mPW1LYP, B3LYP, O3LYP, M06-L, VSXC, HCTH(407), tHCTH, HCTH147, HCTH93, M06-2X, TPSSh.

Here, the results of group 1 yield convincing structures with *RMSE* as small as 0.081 Å in case of the B1B95 functional. It is observed that most of the conventional 5 HGGAs lie in this group as similar as B1B95. The functionals in group 2 yield relatively good structures and the group consists of all 3 LR-HGGAs. For group 3, which exhibits the *RMSE* greater than 0.100 Å, consists of 6 GGAs, and 12 HGGAs. From these investigations, it is apparent that all of the 6 HGGAs functionals designated in group 1 (including B1B95, PBE1PBE, mPW1PBE, mPW1PW91, HSEh1PBE, HSE1PBE) well reproduce the **TS** structures of the MP2 result.

Similarly, the selected geometrical parameters of the product (**2m**) are presented in Figure 2c. The product of MP2 method has an imaginary vibrational frequency (65.23i) with the wiggle of the N–H group. And many attempts to break the imaginary frequency of the product of MP2 were fruitless. But it could not influence the comparison with DFT product. And all of R^2 values are greater than 0.950. The functionals perform in the following order based on the *RMSE* errors:

(a) group 1 (*RMSE* [0.092 Å, 0.099 Å]): B1B95, PBE1PBE, mPW1PBE, mPW1PW91, HSE1PBE, HSEh1PBE, wB97X, B3PW91, CAM-B3LYP, wB97XD, TPSSh;

(b) group 2 (*RMSE* [0.100 Å, 0.109 Å]): tHCTHhyb, B972, BMK, O3LYP, B98, B971;

(c) group 3 (*RMSE* [0.110 Å, 0.192 Å]): tHCTH, M06, B3LYP, M06-L, mPW1LYP, HCTH147, HCTH(407), HCTH93, VSXC, M06-2X.

Similar with the results of **1m** and **TS**, the case of the B1B95 functional in group 1 has the smallest *RMSE* value (0.092 Å) of all functionals. It is observed that most of the conventional 8 HGGAs lie in this group as well as B1B95 result and 3 LR-HGGAs (wB97X, wB97XD, CAM-B3LYP). The functionals in group 2 yield relatively good structures and the group consists of all 6 HGGAs. Group 3, which exhibits the *RMSE* greater than 0.110 Å, consists of the rests functionals. From these investigations, it is apparent that all of the functionals designated in group 1 are suitable to yield equilibrium structures in agreement with the MP2 product structure.

On the basis of the above results, in the aspect of structures, 6 HGGAs functionals (including B1B95, PBE1PBE, mPW1PBE, mPW1PW91, HSEh1PBE, HSE1PBE) can commendably reproduce the structures of MP2.

Thermochemical and Activation Parameters

Secondly, to investigate the mechanism shown in Scheme 1, the relative energy including the corresponding thermal corrections has been computed. As shown in Table 3, ΔE^{++} , ΔG^{++} and ΔH^{++} represent the relative electronic energy, free energy and relative enthalpy of the **TS** with respect to the reactant (**1m**), viz., energy barrier, respectively, and ΔE , ΔG and ΔH are the reaction electronic energy, free energy and enthalpy of the product (**2m** + **NH₃**) with respect to the reactant (**1m**), viz., reaction energy, respectively. And the imaginary frequencies of all **TS**s with several methods are significantly obvious (shown in Table 3). ΔE^{++} (9.51 kcal/mol), ΔG^{++} (9.91 kcal/mol) and ΔH^{++} (9.58 kcal/mol) of DLPNO-CCSD(T) method are more than 1 kcal/mol while ΔE (-26.11 kcal/mol), ΔG (-35.11 kcal/mol) and ΔH (-25.77 kcal/mol) are less than -10 kcal/mol. For PBE1PBE and M06-2X, ΔE^{++} , ΔG^{++} and ΔH^{++} are more than 10

kcal/mol while ΔE , ΔG and ΔH are more than 0 kcal/mol, which causes the N–N bond cleave process is not likely to occur both kinetically and energetically. So PBE1PBE and M06-2X methods could not be suitable to investigate the N–N bond cleave process. Actually, the N–N bond cleave process need to climb the energy barrier in kinetics based on the reliable DLPNO-CCSD(T) results. However, there are 11 functionals (tHCTHhyb, B3LYP, VSXC, HCTH93, wB97X, HCTH147, HCTH(407), O3LYP, M06-L, tHCTH, TPSSh) which ΔE^{++} , ΔG^{++} and ΔH^{++} are less than 1 kcal/mol while ΔE , ΔG and ΔH are less than -10 kcal/mol. And the reactant energy of these methods almost equals to that of transition state and the IRC curve is flat. These results indicate that these methods can't state well the N–N bond cleave process. While the remaining 14 functionals (BMK, B1B95, wB97XD, mPW1PBE, CAM-B3LYP, HSE1PBE, HSEh1PBE, mPW1PW91, M06, B972, B3PW91, B98, mPW1LYP, B971) can reflect the process since ΔE^{++} , ΔG^{++} and ΔH^{++} are more than 1 kcal/mol with ΔE , ΔG and ΔH are less than -10 kcal/mol.

Table 3 . Relative potential energies (kcal/mol, including the corresponding thermal corrections) for stationary points (TS and P(**2m** +NH₃)) with respect to the reactant (**1m**)^a.

method	Energy barrier ΔE^{++}	Energy barrier ΔH^{++}	Energy barrier ΔG^{++}	Reaction energy ΔE	Reaction energy ΔH	Reaction energy ΔG
DLPNO-CCSD(T)	9.51	9.58	9.91	-26.11	-25.77	-35.11
PBE1PBE	76.67	76.76	76.09	48.24	49.02	38.22
M06-2X	18.02	18.08	17.66	14.80	15.41	5.64
BMK	9.84	10.36	8.36	-12.38	-10.85	-23.97
B1B95	6.04	5.65	7.33	-22.76	-22.04	-32.88
wB97XD	6.63	6.63	7.33	-17.61	-16.66	-27.80
mPW1PBE	4.13	3.69	5.04	-25.57	-24.77	-35.67
CAM-B3LYP	5.61	5.79	4.85	-20.21	-19.38	-30.31
HSE1PBE	4.04	4.13	3.49	-24.65	-23.86	-34.71
HSEh1PBE	4.03	4.13	3.46	-24.66	-23.87	-34.71
mPW1PW91	4.00	4.13	3.27	-25.77	-24.96	-35.94
M06	3.40	3.46	3.26	-24.59	-23.86	-34.59
B972	2.43	2.54	1.86	-32.44	-31.55	-42.90
B3PW91	2.13	2.18	1.82	-32.49	-31.65	-42.79
B98	1.79	1.83	1.63	-30.13	-29.34	-40.41
mPW1LYP	2.06	2.14	1.54	-27.17	-26.38	-37.25
B971	1.68	1.76	0.88	-30.04	-29.24	-40.39
tHCTHhyb	0.44	0.42	0.42	-35.71	-34.84	-46.46
B3LYP	0.81	0.83	0.37	-34.00	-33.16	-44.47
VSXC	-0.06	-0.14	0.10	-32.51	-31.23	-43.55
HCTH93	-0.47	-0.75	0.09	-54.85	-53.89	-65.39
TPSSh	0.02	-0.13	0.03	-37.67	-36.92	-47.39
wB97X	0.00	0.00	0.00	-23.45	-22.70	-33.18
HCTH147	-0.41	-0.73	-0.05	-50.43	-49.55	-60.80
HCTH(407)	-0.47	-0.66	-0.09	-50.17	-49.13	-60.84
O3LYP	0.18	0.25	-0.21	-43.71	-42.77	-54.44
M06-L	-0.18	-0.02	-1.02	-38.84	-38.05	-49.18
tHCTH	-0.35	-0.10	-2.16	-48.67	-47.12	-61.53

^a ΔG^{++} and ΔH^{++} represent the relative free energy and relative enthalpy of the **TS** with respect to the reactant (**1m**), respectively, and ΔG and ΔH are the reaction free energy and enthalpy of the product (**2m**) with respect to the reactant (**1m**), respectively.

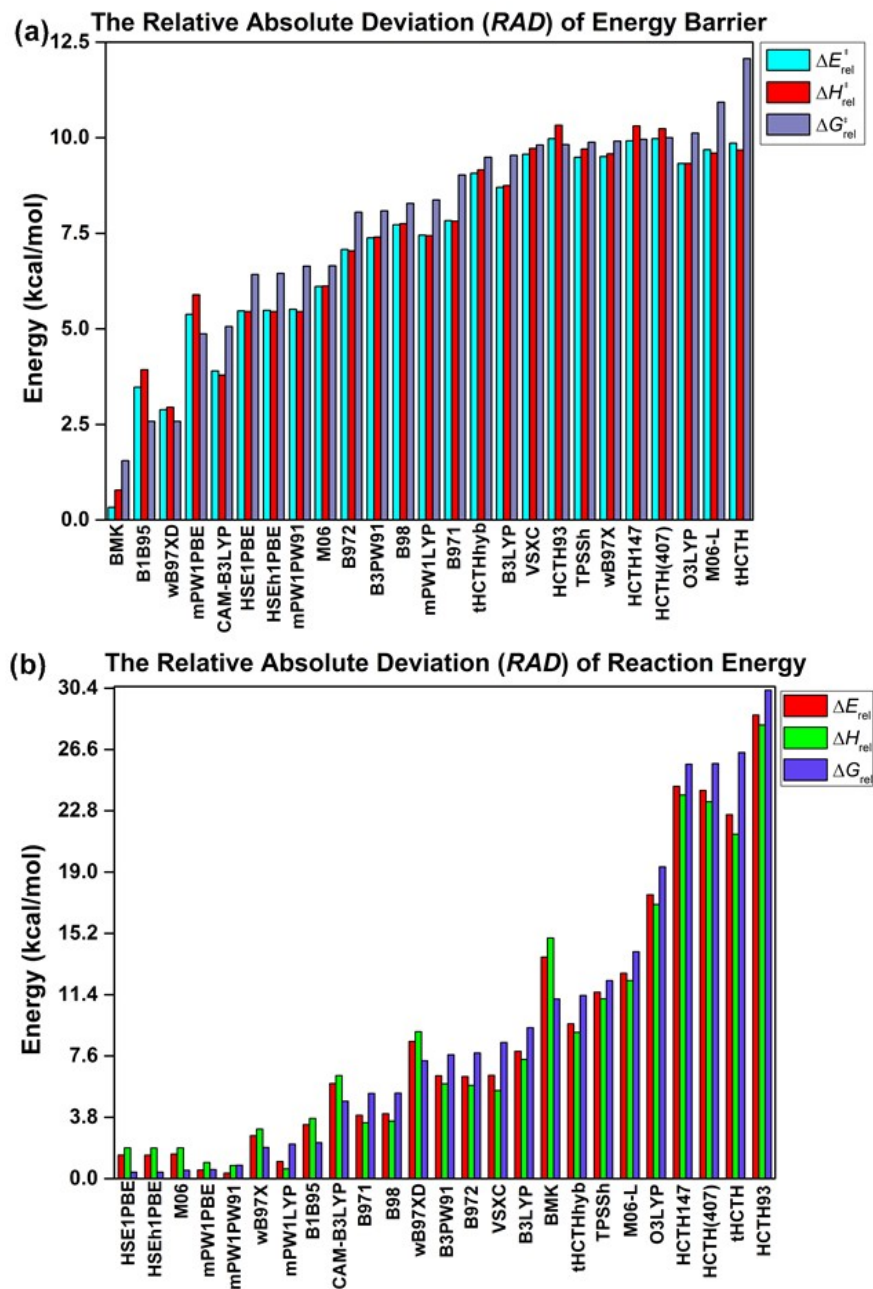


Figure 3 . The *RAD* (relative absolute deviation, kcal/mol) of energy barrier (a) and reaction energy (b) compared with the results of DLPNO-CCSD(T) level. Since the results of PBE1PBE and M06-2X methods are far off that of DLPNO-CCSD(T), they could not be included in this figure.

Similarly, as the statistics of optimized geometries, the energy barrier and reaction energy are shown in Figure 3. As shown in Figure 3a, in the respect of energy barrier, according to Gibbs free energy, the functionals *RAD* (relative absolute deviation, kcal/mol, represents the absolute values of difference) of energy barrier compared with the results of DLPNO-CCSD(T) level, which is arranged from small to big, is divided into several groups in the following order:

- (a) group 1 (*RAD* [1.55 kcal/mol, 2.58 kcal/mol]): BMK, B1B95, wB97XD;
- (b) group 2 (*RAD* [4.87 kcal/mol, 5.06 kcal/mol]): mPW1PBE, CAM-B3LYP;
- (c) group 3 (*RAD* [6.42 kcal/mol, 8.37 kcal/mol]): HSE1PBE, HSEh1PBE, mPW1PW91, M06, B972, B3PW91, B98, mPW1LYP;
- (d) group 4 (*RMSE* [9.03 kcal/mol, 12.07 kcal/mol]): B971, tHCTHhyb, B3LYP, VSXC, HCTH93, TPSSh, wB97X, HCTH147, HCTH(407), O3LYP, M06-L, tHCTH.

These results indicate that the energy barrier from the three functionals (BMK, B1B95 and wB97XD) are very close to that of DLPNO-CCSD(T) method within 3 kcal/mol.

For comparison of the reaction energy, shown in Figure 3b, according to Gibbs free energy, the functionals *RAD* compared with the results of DLPNO-CCSD(T) level, is divided into several groups in the following order:

- (a) group 1 (*RAD* [0.40 kcal/mol, 2.23 kcal/mol]): HSE1PBE, HSEh1PBE, M06, mPW1PBE, mPW1PW91, wB97X, mPW1LYP, B1B95;
- (b) group 2 (*RAD* [4.80 kcal/mol, 5.30 kcal/mol]): CAM-B3LYP, B971, B98;
- (c) group 3 (*RAD* [7.31 kcal/mol, 8.44 kcal/mol]): wB97XD, B3PW91, B972, VSXC;
- (d) group 4 (*RMSE* [9.36 kcal/mol, 30.28 kcal/mol]): B3LYP, BMK, tHCTHhyb, TPSSh, M06-L, O3LYP, HCTH147, HCTH(407), tHCTH, HCTH93.

These classifications indicate that the eight functionals (HSE1PBE, HSEh1PBE, M06, mPW1PBE, mPW1PW91, wB97X, mPW1LYP and B1B95) of group 1 have the more satisfactory results in comparison with that of DLPNO-CCSD(T) method within 3 kcal/mol.

So in the respect of thermochemical and activation parameters (including the energy barrier and reaction energy), the three functionals (B1B95, mPW1PBE and CAM-B3LYP) are consistent with the DLPNO-CCSD(T) result which the differences are within 5.06 kcal/mol. Then, the differences of HSE1PBE and HSEh1PBE functionals are within 6.45 kcal/mol followed.

Here, we summarize these results with the following remarks:

- (i) In the process of search of transition states using various DFT methods for N–N bond cleave process, eighteen DFT methods (BP86, B97D, PBEPBE, BLYP, mPWPW91, PW91PW91, TPSSTPSS, B3P86, mPW3PBE, B1LYP, X3LYP, BHandH, BHandLYP, HSE2PBE, PBEh1PBE, M06HF, wB97, LC-WPBE) can't locate successfully transition states. This shows that these are not suitable for N-N bond fracture system.
- (ii) For the structure of diiron complexes, six HGGAs (B1B95, PBE1PBE, mPW1PBE, mPW1PW91, HSEh1PBE, HSE1PBE) can reproduce the geometries of MP2 method. And the B1B95 functional is best for structures.
- (iii) For in the respect of the relative energy, the five functionals (B1B95, mPW1PBE, CAM-B3LYP, HSE1PBE and HSEh1PBE) are consistent with the DLPNO-CCSD(T) results which the differences are within 6.45 kcal/mol. And the B1B95 functionals has the smallest energy difference within 3 kcal/mol of the DLPNO-CCSD(T) data.

Conclusions

By computationally modelling the reaction of a diiron-mediated N–N bond cleavage (the decomposition reaction of complex $\text{Cp}^*\text{Fe}(\mu\text{-SEt})_2(\mu\text{-NHNH}_3)\text{FeCp}^*$ ($\text{Cp}^* = \eta^5\text{-C}_5\text{Me}_5, \mathbf{1}$) to $\text{Cp}^*\text{Fe}(\mu\text{-SEt})_2(\mu\text{-NH})\text{FeCp}^*$ ($\mathbf{2}$) and NH_3), a wide range of DFT functionals have been performed for the benchmark study compared with the higher level MP2 and DLPNO-CCSD(T) results. The DFT benchmarks show that the HGGGA functional

of B1B95 is the best functional among all of the benchmarked DFT functionals for the structures and relative energies. The reliability of these three functionals (mPW1PBE, HSE1PBE and HSEh1PBE) follows the B1B95. This work can help better choosing reasonable DFT functional to study the N–N bond cleavage of dinuclear clusters.

Supplementary Material

Supplementary data associated with this article can be found, in the online version, at <http://dx.doi.org/>.

Author Information

Corresponding Author

E-mail: luolun@hbmhu.edu.cn (L. L.).

Notes

The authors declare no competing financial interest.

Acknowledgements

This work was supported by the Cultivating Project for Young Scholar at Hubei University of Medicine (2018QDJZR13 for L. L.).

References

- [1] (a) Chatt, J.; Dilworth, J. R.; Richards, R. L. *Chem. Rev.* **1978**, *78*, 589–625. (b) Leigh, G. J.; Jimenez-Tenorio, M. *J. Am. Chem. Soc.* **1991**, *113*, 5862–5863. (c) Barney, B. M.; Lee, H. -I.; Dos Santos, P. C.; Hoffman, B. M.; Dean, D. R.; Seefeldt, L. C. *Dalton Trans.* **2006**, 2277–2284. (d) Barney, B. M.; Lukoyanov, D.; Yang, T. -C.; Dean, D. R.; Hoffman, B. M.; Seefeldt, L. C. *Proc. Natl. Acad. Sci. U. S. A.* **2006**, *103*, 17113–17118. (e) Dance, I. *Dalton Trans.* **2008**, 5977–5991. (f) Sokolov, A. Y.; Schaefer, H. F. *Organometallics* **2010**, *29*, 3271–3280.
- [2] (a) Hoffman, B. M.; Dean, D. R.; Seefeldt, L. C. *Acc. Chem. Res.* **2009**, *42*, 609–619. (b) Hu, Y.; Ribbe, M. W. *Acc. Chem. Res.* **2010**, *43*, 475–484.
- [3] (a) Deng, H.; Hoffmann, R. *Angew. Chem., Int. Ed.* **1993**, *32*, 1062–1065. (b) Zhong, S. -J.; Liu, C. -W. *Polyhedron* **1997**, *16*, 653–661. (c) Stavrev, K. K.; Zerner, M. C. *Theor. Chem. Acc.* **1997**, *96*, 141–145. (d) Dance, I. *Chem. Commun.* **1998**, 523–530. (e) Siegbahn, P. E. M.; Westerberg, J.; Svensson, M.; Crabtree, R. H. *J. Phys. Chem. B* **1998**, *102*, 1615–1623. (f) Rod, T. H.; Hammer, B.; Nørskov, J. K. *Phys. Rev. Lett.* **1999**, *82*, 4054–4057. (g) Dos Santos, P. C.; Dean, D. R.; Hu, Y.; Ribbe, M. W. *Chem. Rev.* **2004**, *104*, 1159–1173. (h) Barney, B. M.; McClead, J.; Lukoyanov, D.; Laryukhin, M.; Yang, T. -C.; Dean, D. R.; Hoffman, B. M.; Seefeldt, L. C. *Biochemistry* **2007**, *46*, 6784–6794. (i) Kastner, J.; Blochl, P. E. *J. Am. Chem. Soc.* **2007**, *129*, 2998–3006. (j) Xie, H.; Wu, R.; Zhou, Z.; Cao, Z. *J. Phys. Chem. B* **2008**, *112*, 11435–11439. (k) Tanaka, H.; Mori, H.; Seino, H.; Hidai, M.; Mizobe, Y.; Yoshizawa, K. *J. Am. Chem. Soc.* **2008**, *130*, 9037–9047.
- [4] Perdew, J. P.; Burke, K.; Ernzerhof, M. *Phys. Rev. Lett.* **1996**, *77*, 3865–3868.
- [5] (a) Perdew, J. P.; Wang, Y. *Phys. Rev. B* **1992**, *45*, 13244–13249. (b) Perdew, J. P.; Chevary, J. A.; Vosko, S. H.; Jackson, K. A.; Pederson, M. R.; Singh, D. J.; Fiolhais, C. *Phys. Rev. B* **1992**, *46*, 6671–6687.
- [6] (a) Chen, Y.; Zhou, Y.; Chen, P.; Tao, Y.; Li, Y.; Qu, J. *J. Am. Chem. Soc.* **2008**, *130*, 15250–15251. (b) Chen, Y.; Liu, L.; Peng, Y.; Chen, P.; Luo, Y.; Qu, J. *J. Am. Chem. Soc.* **2011**, *133*, 1147–1149. (c) Luo, Y.; Li, Y.; Yu, H.; Zhao, J.; Chen, Y.; Hou, Z. Qu, J. *Organometallics* **2012**, *31*, 335–344.
- [7] Tao, J. M.; Perdew, J. P.; Staroverov, V. N.; Scuseria, G. E. *Phys. Rev. Lett.* **2003**, *91*, 146401.
- [8] Møller, C.; Plesset, M. S. *Phys. Rev.* **1934**, *46*, 618–622.

- [9] Frisch, M. J. et al. *Gaussian 09*, Revision A.02, Gaussian, Inc., Wallingford CT, 2009. See Supplementary Material for full citation of this program.
- [10] Riplinger, C.; Neese, F. *J. Chem. Phys.* **2013**, *138*, 034106.
- [11] Riplinger, C.; Sandhoefer, B.; Hansen, A.; Neese, F. *J. Chem. Phys.* **2013**, *139*, 134101.
- [12] Neese, F. *Wiley Interdiscip. Rev.: Comput. Mol. Sci.* **2012**, *2*, 73–78.
- [13] (a) Svensson, M.; Humbel, S.; Froese, R. D. J.; Matsubara, T.; Sieber, S.; Morokuma, K. *J. Phys. Chem.* **1996**, *100*, 19357–19363. (b) Maseras, F.; Morokuma, K. *J. Comput. Chem.* **1995**, *16*, 1170–1179. (c) Vreven, T.; Morokuma, K. *J. Comput. Chem.* **2000**, *21*, 1419–1432.
- [14] (a) Becke, A. D. *Phys. Rev. A* **1988**, *38*, 3098–3100. (b) Perdew, J. P. *Phys. Rev. B* **1986**, *33*, 8822–8824. (c) Becke, A. D. *J. Chem. Phys.* **1993**, *98*, 5648–5652.
- [15] Hamprecht, F. A.; Cohen, A. J.; Tozer, D. J.; Handy, N. C. *J. Chem. Phys.* **1998**, *109*, 6264–6271.
- [16] Grimme, S. *J. Comput. Chem.* **2006**, *27*, 1787–1799.
- [17] Lee, C. T.; Yang, W. T.; Parr, R. G. *Phys. Rev. B* **1988**, *37*, 785–789.
- [18] Adamo, C.; Barone, V. *J. Chem. Phys.* **1998**, *108*, 664–675.
- [19] Van Voorhis, T.; Scuseria, G. E. *J. Chem. Phys.* **1998**, *109*, 400–410.
- [20] Boese, A. D.; Handy, N. C. *J. Chem. Phys.* **2002**, *116*, 9559–9569.
- [21] (a) Zhao, Y.; Truhlar, D. G. *Acc. Chem. Res.* **2008**, *41*, 157–167. (b) Zhao, Y.; Truhlar, D. G. *J. Chem. Phys.* **2006**, *125*, 194101.
- [22] Stephens, P. J.; Devlin, F. J.; Chabalowski, C. F.; Frisch, M. J. *J. Phys. Chem.* **1994**, *98*, 11623–11627.
- [23] (a) Schmider, H. L.; Becke, A. D. *J. Chem. Phys.* **1998**, *108*, 9624–9631. (b) Becke, A. D. *J. Chem. Phys.* **1997**, *107*, 8554–8560.
- [24] Perdew, J. P. Unified Theory of Exchange and Correlation Beyond the Local Density Approximation. In *Electronic Structure of Solids*, in: P. Zieche, H. Eschrig (Eds.), Berlin, Germany, 1991, pp. 11–20.
- [25] Wilson, P. J.; Bradley, T. J.; Tozer, D. J. *J. Chem. Phys.* **2001**, *115*, 9233–9242.
- [26] Becke, A. D. *J. Chem. Phys.* **1996**, *104*, 1040–1046.
- [27] (a) Handy, N. C.; Cohen, A. J. *Mol. Phys.* **2001**, *99*, 403–412. (b) Hoe, W. M.; Cohen, A. J.; Handy, N. C. *Chem. Phys. Lett.* **2001**, *341*, 319–328.
- [28] Xu, X.; Goddard, W. A. *Proc. Natl. Acad. Sci. U.S.A.* **2004**, *101*, 2673–2677.
- [29] Henderson, T. M.; Izmaylov, A. F.; Scalmani, G.; Scuseria, G. E. *J. Chem. Phys.* **2009**, *131*, 044108.
- [30] (a) Heyd, J.; Scuseria, G. E.; Ernzerhof, M. *J. Chem. Phys.* **2006**, *124*, 219906. (b) Paier, J.; Marsman, M.; Hummer, K.; Kresse, G.; Gerber, I. C.; Angyan, J. G. *J. Chem. Phys.* **2006**, *125*, 249901.
- [31] Heyd, J.; Scuseria, G. E.; Ernzerhof, M. *J. Chem. Phys.* **2003**, *118*, 8207–8215.
- [32] Ernzerhof, M.; Scuseria, G. E. *J. Chem. Phys.* **1999**, *110*, 5029–5036.
- [33] Boese, A. D.; Martin, J. M. L. *J. Chem. Phys.* **2004**, *121*, 3405–3416.
- [34] Zhao, Y.; Truhlar, D. G. *Theor. Chem. Acc.* **2008**, *120*, 215–241.
- [35] Zhao, Y.; Truhlar, D. G. *J. Phys. Chem. A* **2006**, *110*, 13126–13130.
- [36] Staroverov, V. N.; Scuseria, G. E.; Tao, J.; Perdew, J. P. *J. Chem. Phys.* **2003**, *119*, 12129–12137.

- [37] Boese, A. D.; Handy, N. C. *J. Chem. Phys.* . **2002** , *116* , 9559–9569.
- [38] Chai, J. D.; Head-Gordon, M. *J. Chem. Phys.* .**2008** , *128* , 084106.
- [39] Chai, J. D.; Head-Gordon, M. *Phys. Chem. Chem. Phys.* .**2008** , *10* , 6615–6620.
- [40] Tawada, Y.; Tsuneda, T.; Yanagisawa, S.; Yanai, T.; Hirao, K. *J. Chem. Phys.* . **2004** , *120* , 8425–8433.
- [41] Yanai, T.; Tew, D. P.; Handy, N. C. *Chem. Phys. Lett.* . **2004** , *393* , 51–57.